Surface and bulk ferroelectric phase transition in super-tetragonal $BiFeO_3$ thin films

Myriam Lachheb,[1] Qiuxiang Zhu,[2] Stéphane Fusil,[2,3,*] Qiang Wu,[1,†] Cécile Carrétéro,[2] Aymeric Vecchiola,[2] Manuel Bibes,[2] Dominique Martinotti,[1] Claire Mathieu,[1] Christophe Lubin,[1] Alexandre Pancotti,[4] Xiaoyan Li-Bourrelier,[5] Alexandre Gloter,[5] Brahim Dkhil,[6] Vincent Garcia,[2] and Nick Barrett[1,‡]

[1]*SPEC, CEA, CNRS, Université Paris-Saclay, CEA Saclay, 91191 Gif-sur-Yvette, France*
[2]*Unité Mixte de Physique, CNRS, Thales, Université Paris-Saclay, 91767 Palaiseau, France*
[3]*Université d'Evry, Université Paris-Saclay, 91000 Evry, France*
[4]*Federal University of Goias, Unidade Academica Especial de Ciencias Exactas e Tecnologicas, Campus Jatoba - Ciudade Universitaria, BR 364 km 195 3800, 75801-615, Jatai-GO, Brazil*
[5]*Laboratoire de Physique des Solides, CNRS, Université Paris-Saclay, 91405 Orsay, France*
[6]*Laboratoire Structures, Propriétés et Modélisation des Solides, CentraleSupélec, CNRS-UMR8580, Université Paris-Saclay, 91190 Gif-sur-Yvette, France*

(Received 2 November 2020; revised 20 January 2021; accepted 4 February 2021; published 23 February 2021)

The temperature-dependent ferroelectric properties of super-tetragonal $BiFeO_3$ are investigated using surface-sensitive low-energy electron microscopy (LEEM). We use epitaxial oxide $BiFeO_3/Ca_{0.96}Ce_{0.04}MnO_3$ bilayers grown by pulsed laser deposition on $YAlO_3$ substrates. Ferroelectric, micrometer-scale domains are written by piezoresponse force microscopy and subsequently observed by LEEM from room temperature up to about 950 K. Kelvin probe force microscopy and LEEM spectroscopy reveal that the surface potential is efficiently (>50%) screened by adsorbates that are only released after annealing above 873 ± 50 K in ultrahigh vacuum. The surface structure and chemistry of the ferroelectric thin films are analyzed using scanning transmission electron microscopy, electron energy loss spectroscopy, and x-ray photoelectron spectroscopy, discarding the occurrence of a putative "skin layer" effect. While its magnetic and structural transitions were reported in the literature, the true, ferroelectric Curie temperature of super-tetragonal $BiFeO_3$ has not been determined so far. Here, we measure a Curie temperature of 930 ± 30 K for the super-tetragonal $BiFeO_3$ surface and corroborate it with volume-sensitive, temperature-dependent x-ray diffraction measurements. These results suggest that LEEM can be used as a powerful tool to probe surface charge and ferroelectric transitions in ultrathin films.

DOI: 10.1103/PhysRevMaterials.5.024410

I. INTRODUCTION

Bismuth ferrite ($BiFeO_3$) is a room-temperature, multiferroic material that crystallizes in the *R*3*c* space group with a Curie temperature of 1100 K and a Néel temperature of 640 K [1–3]. Given its multiple assets such as a high ferroelectric polarization (100 $\mu C/cm^2$) [4] and the coupling between ferroelectric and antiferromagnetic orders [5], $BiFeO_3$ has been intensively investigated over the last two decades [6]. In this context, the discovery of a highly distorted ferroelectric phase in $BiFeO_3$ [7] with the highest expected ferroelectric polarization (up to 150 $\mu C/cm^2$) [8,9] opens new perspectives. Indeed, high compressive strain in epitaxial thin films triggers a structural transition from the rhombohedral ($c/a \sim 1.03$, R-$BiFeO_3$) ground state to the so-called super-tetragonal polymorph ($c/a \sim 1.23$, T-$BiFeO_3$) [10]. The genuine assets of T-$BiFeO_3$ make it an appealing functional ingredient to explore new device concepts. The existence of a morphotropic phase boundary between the rhombohedral-like R and T phases offers possibilities for large piezoresponse [11] and reversible electrochromism [12]. Furthermore, ultrathin films of pure super-tetragonal $BiFeO_3$ show a large tunnel electroresistance associated with polarization reversal [13] and can be used as artificial synapses for neuromorphic computing [14].

While the ferroelectric character of bulk R-$BiFeO_3$ derives mainly from the movement of Bi atoms, both Bi and Fe contribute to the higher polarization values in the highly strained T-$BiFeO_3$ [8]. The off-centering in the Fe-O bond along [001] in the T phase is twice that along [111] in the R phase. The polarization contributions are 80 and 55 $\mu C/cm^2$ for Bi-O and Fe-O distortions, respectively. In addition, structural transitions of T-$BiFeO_3$ thin films from monoclinic M_C to monoclinic M_A [corresponding to polarization in the (110) and (100) pseudocubic planes, respectively] and then to a purely tetragonal T phase when increasing temperature are detected using x-ray diffraction [15–17]. In mixed R and T phase thin films of $BiFeO_3$ grown on $LaAlO_3$ substrates, the M_C-M_A transition occurs at 373 K [15,17], and the M_A-T transition is observed at 703 K [15]. In pure T-$BiFeO_3$ thin films grown on $YAlO_3$, the M_C-M_A transition is detected in the same temperature range (423 K), while the M_A-T transition happens at a much lower temperature (548 K)

*Corresponding author: Stephane.fusil@cnrs-thales.fr
†Present address: Department of Earth Sciences, The University of Hong Kong, Hong Kong.
‡Corresponding author: nick.barrett@cea.fr

[16]. In addition, although the M_A-T transition is supposedly attributed to the Curie temperature of super-tetragonal $BiFeO_3$ [10], Raman spectroscopy indicates that the high-temperature tetragonal phase is still polar, and a Curie temperature of 1140 ± 100 K is extrapolated from the decay of this Raman mode [15]. All these results suggest that the ferroelectric properties of T-$BiFeO_3$ are more complex and potentially more sensitive to strain than those of its parent material. In addition, the influence of the surface on the temperature-induced phase transitions in T-$BiFeO_3$ films was not addressed. This issue is particularly relevant as the T-$BiFeO_3$ polymorph only exists in the form of epitaxially strained thin films. The typical thickness ensuring purely T phase and no relaxation is a few tens of nanometers. At this scale, efficient screening is required to compensate bound surface polarization charges and maintain ferroelectricity. On bare surfaces, chemisorption of polar molecules may provide an efficient screening mechanism [18–20], and surface chemistry is crucial to understand the ferroelectric properties of such thin films [21]. Indeed, it has been suggested that the electrochemistry of ionic adsorption is inseparable from the ferroelectric character of a surface [22]. Physisorption or chemisorption can drastically change the boundary conditions of the ferroelectric $BiFeO_3$ film and could result in polarization pinning and modulation of the phase diagram since phase transitions often start from the surface. Super-tetragonality has also been linked to the presence of a substoichiometric, Bi oxide surface layer [23]. Then, surface chemistry may be a key parameter governing the ferroelectric behavior of super-tetragonal $BiFeO_3$ thin film that remains to be explored. Indeed, the surface or interface boundary conditions appear to influence the polarization switching [24].

Here, we employ multiple microscopy techniques to assess the temperature-dependent ferroelectric properties of super-tetragonal $BiFeO_3$ thin films. Using piezoresponse force microscopy, we first detect the pristine polarization state of the films and measure local piezoelectric hysteresis loops. Second, we write the micrometer-sized domain with upward and downward polarizations. The surface potential of these domains is assessed by ambient-room-temperature Kelvin probe force microscopy. We use variable-temperature, surface-sensitive low-energy electron microscopy to probe local variations in the surface potential at the surface of microscopic domains [25,26]. Finally, the surface chemistry is analyzed using x-ray photoemission spectroscopy and atomically resolved scanning transmission electron microscopy with electron energy loss spectroscopy.

II. FILM GROWTH AND STRUCTURAL PROPERTIES

Epitaxial $BiFeO_3/Ca_{0.96}Ce_{0.04}MnO_3$ oxide heterostructures are fabricated by pulsed laser deposition on $YAlO_3$ (001) substrates using a tripled-frequency Nd:YAG laser. The 20-nm-thick $Ca_{0.96}Ce_{0.04}MnO_3$ layer, grown at 943 K under an oxygen pressure of 20 Pa, is used as a bottom electrode to switch the polarization of $BiFeO_3$. The 25-nm-thick $BiFeO_3$ layer is subsequently grown at 853 K under an oxygen pressure of 0.6 Pa. The sample is then cooled down to room temperature under high oxygen pressure (3×10^4 Pa) to avoid the formation of oxygen vacancies. The film thickness and topography are determined using x-ray reflectivity and atomic force microscopy, respectively. The $BiFeO_3$ films show flat surfaces with a root-mean-square roughness of less than 0.5 nm, without any lamellar features characteristic of mixed phases [15]. 2θ-ω diffraction scans show that $BiFeO_3$ is purely in the super-tetragonal phase and does not contain any parasitic or rhombohedral-like phases [Fig. 1(a)]. Laue fringes around the (001) peak of $BiFeO_3$ attest to the coherent growth of the films. The calculated out-of-plane parameter is 0.4653 nm, in agreement with reported values from the literature [10]. Reciprocal space mappings around the asymmetric $YAlO_3$ (206), (116), (026), and (116) peaks indicate that the $BiFeO_3$ is not fully strained by the substrate [as illustrated in Fig. 1(b) for $YAlO_3$ (116)] with an estimated in-plane lattice constant of 0.379(5) nm. This leads to a c/a value of 1.225 and a volume of 0.067 nm^3, as typically observed for this super-tetragonal polymorph [10].

III. ROOM-TEMPERATURE SURFACE PROPERTIES

The cross-section microstructure of the as-grown $BiFeO_3$ thin film on $YAlO_3$ is investigated in a NION UltraSTEM200 C3/C5-corrected scanning transmission electron microscope (STEM), using atomically resolved high-angle annular dark-field imaging (HAADF). The corresponding near-surface chemical mapping was studied by electron energy loss spectroscopy (EELS) spectrum image [Fig. 1(d)]. The HAADF-STEM observations confirm the high distortion of the $BiFeO_3$ unit cell with a constant giant tetragonality ($c/a = 1.25 \pm 0.03$) up to the surface and no traces of rhombohedral-like $BiFeO_3$. From the off-centering of the Fe cation, we deduce that the pristine polarization points downward, i.e., towards the oxide electrode. The EELS fine-structure analysis indicates that the $BiFeO_3$ surface is $(BiO)^+$ terminated and that the 3+ Fe valency does not change at the surface [Fig. 1(e)]. Thus there is no evidence for a chemically altered "skin layer" [27] at the surface of the super-tetragonal $BiFeO_3$ film.

Piezoresponse force microscopy (PFM) experiments are conducted with an atomic force microscope (Nanoscope V Multimode; Bruker). An ac external source (DS360; Stanford Research) operating at 35 kHz is connected to the bottom electrode while the tip is grounded. An external lock-in (SR830; Stanford Research) is used for the acquisition of the out-of-plane piezoresponse. The local piezoelectric hysteresis loop [Fig. 1(c)] has a positive bias imprint ($E_{imprint} \sim 400$ kV/cm), in accordance with the virgin downward ferroelectric state observed by PFM imaging and HAADF-STEM. Figure 2(a) shows a typical out-of-plane PFM phase image of the $BiFeO_3$ thin film, in which squares of different sizes (1×1 μm^2 to 20×20 μm^2) were written by scanning the surface with a positive dc voltage of 8 V applied to the bottom electrode (about twice the coercive field value). The bright and dark contrast correspond to the downward and upward polarization states, respectively, with the expected 180° phase contrast between them.

The low-energy electron microscopy (LEEM) experiments were done in an Elmitec-III MEM-LEEM ultrahigh vacuum (UHV, base pressure 2×10^{-8} Pa) system. The field of view is 75 μm with a spatial resolution of 15 nm. The incident

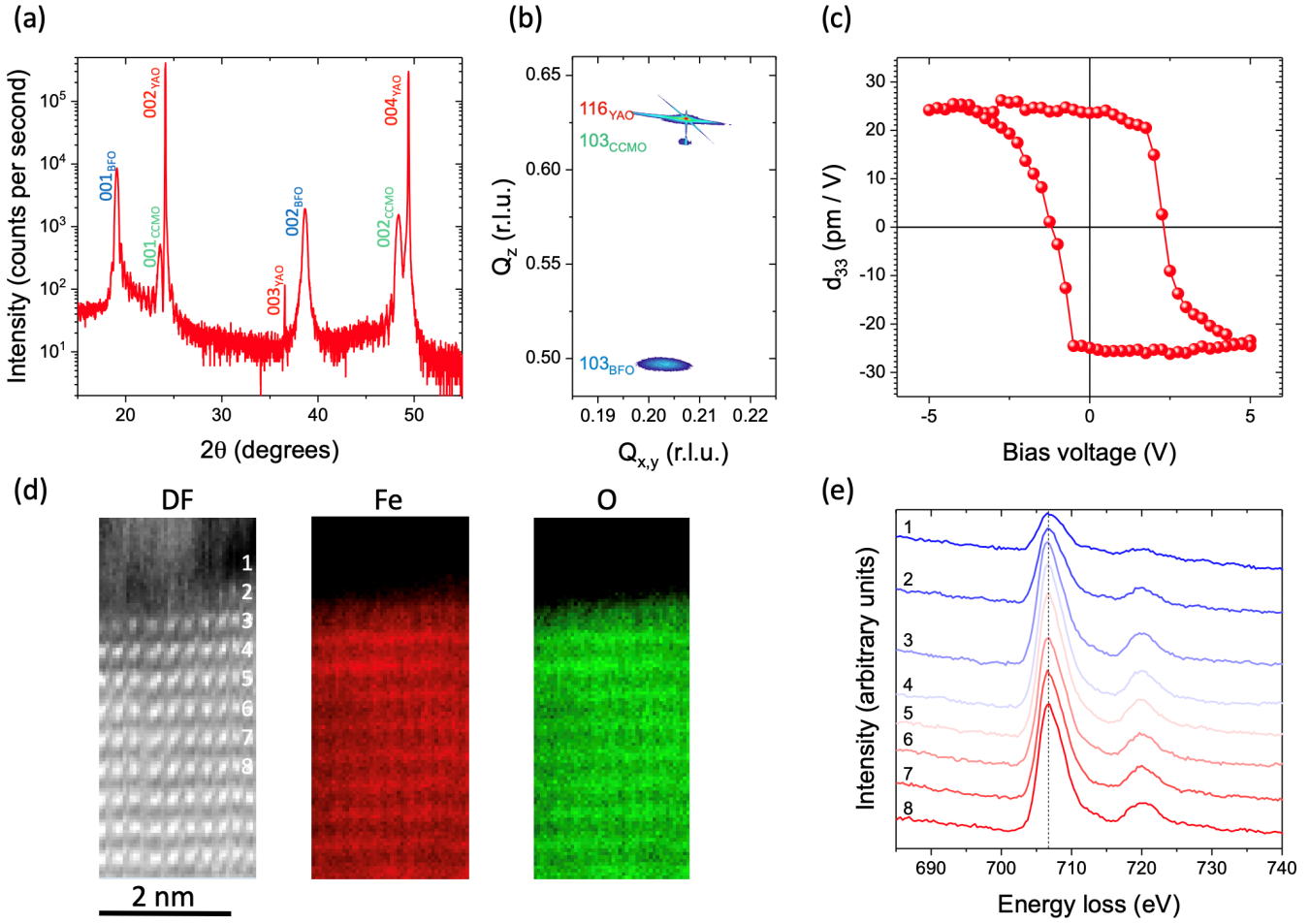

FIG. 1. (a) 2θ-ω x-ray diffraction scan of a $BiFeO_3$ thin film on $Ca_{0.96}Ce_{0.04}MnO_3/YAlO_3$ (001). (b) Reciprocal space mapping around the $YAlO_3$ (116) peak. These structural characterizations indicate that $BiFeO_3$ is only in its super-tetragonal phase. (c) Local piezoelectric loop as a function of the bias voltage applied to the $Ca_{0.96}Ce_{0.04}MnO_3$ electrode. The imprint to the right indicates a preferential downward polarization orientation. (d) Dark-field (DF) and electron energy loss spectroscopy images at the Fe and O edges. (e) Spectra at the Fe L edge showing that the Fe valence is not modified at the surface. BFO, $BiFeO_3$; CCMO, $Ca_{0.96}Ce_{0.04}MnO_3$; r.l.u., reciprocal lattice units; YAO, $YAlO_3$.

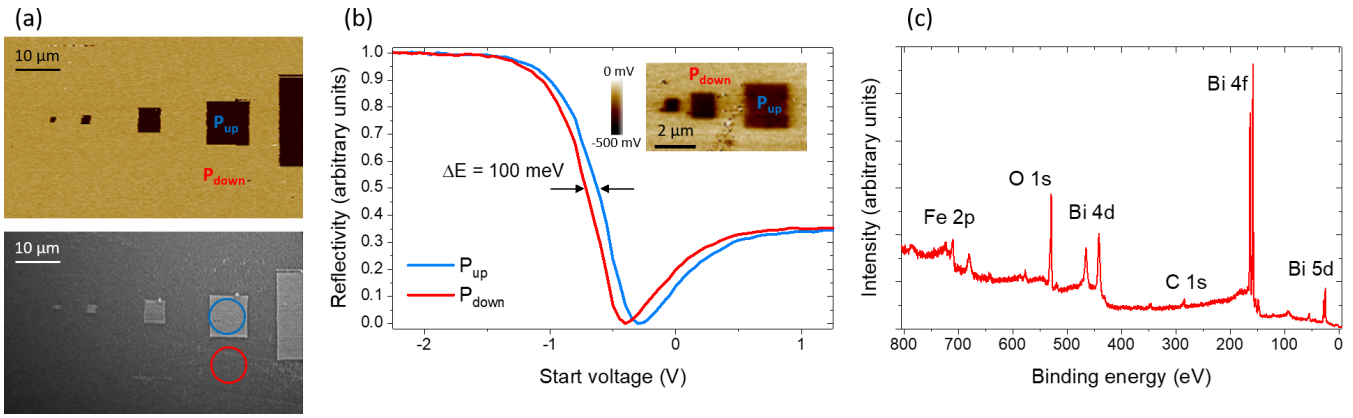

FIG. 2. (a) Room-temperature detection of ferroelectric domains using PFM (top) and MEM (bottom) at a start voltage of −0.95 V. (b) Electron reflectivity as a function of the start voltage showing the MEM-LEEM transition for up and down ferroelectric domains. In the inset, KPFM surface potential image at the $BiFeO_3$ surface on an area where upward ferroelectric domains were preliminary written. The up domains show a lower electrostatic surface potential than pristine down domains. (c) X-ray photoemission spectroscopy showing the presence of 0.1 monolayer of carbon contamination.

electron energy, called the start voltage (SV), is defined by the sample bias with respect to the work function of the electron gun. Detector and illumination inhomogeneities were removed by normalization using an image acquired from a uniform part of the sample surface (so-called flat field normalization). The LEEM image of the same domain structure is shown in the lower panel of Fig. 2(a) under SV = −0.95 V. The intensity contrast reflects a difference in reflectivity, the written domains having a higher reflectivity than the as-deposited film. Figure 2(b) plots the electron reflectivity as a function of SV from the upward domains and the surrounding as-grown film with downward polarization. At very low incident energy, electrons are reflected [mirror electron microscopy (MEM)], whereas at higher energy they overcome the surface potential barrier to penetrate the first layers of the sample surface and are backscattered (true LEEM). The surface potential, given by the position of the MEM-LEEM transition, is shifted (100 ± 20) meV to higher energy for the upward domains (blue curve) with respect to that of the as-grown film (red curve). This is the opposite to what is expected from a surface with unscreened polarization charge.

This surface potential has also been measured using Kelvin probe force microscopy (KPFM) in air (Bruker Icon). The result is included as an inset in Fig. 2(b). The KPFM image indicates that the written domains with upward polarization show a lower surface potential than the surrounding as-grown film. This is also contrary to the expected surface potential of an unscreened ferroelectric surface, which should be high (low) for upward (downward) polarized domains [28,29]. Hence this inverted surface potential suggests that an efficient screening occurs at the ferroelectric surface of $BiFeO_3$. STEM-EELS investigations were performed on a cross section of written domains with upward polarization. The layer-by-layer analysis indicates no modification of the Fe valence state from the bulk to the surface of the film, as observed for the as-grown state [Fig. 1(d)]. The results agree with x-ray absorption measurements using linearly polarized light along the *c* axis which show an $L_{2,3}$ absorption edge typical of the Fe^{3+} valence state [8]. Thus the surface potential difference observed in Figs. 2(a) and 2(b) is not due to differences in the surface chemistry of $BiFeO_3$ but can only be ascribed to polarization. Nevertheless, this is in contradiction to the simple picture as the upward polarization, or positive surface polarization bound charge, should give rise to a MEM-LEEM transition at lower start voltage [26,30]. Indeed, both LEEM microscopy and KPFM data, acquired under UHV and ambient atmosphere, respectively, exhibit a potential contrast [Figs. 2(a) and 2(b)] opposite to that expected assuming bare $BiFeO_3$ surfaces. We conclude that this contrast inversion reflects the adsorption of chemisorbed polar molecules, which provide near-complete screening of surface bound charges. The incident electrons in LEEM and the KPFM tip therefore both probe surface charge opposite to that associated with unscreened surface polarization.

To further investigate the surface chemical properties of the films, we performed x-ray photoemission spectroscopy (XPS) measurements using a monochromatic Al K_α source (1486.7 eV) and an Argus-128 hemispherical analyzer (Scienta Omicron). The pass energy of 20 eV gives an overall energy resolution of 0.3 eV. These measurements are done at room temperature at a base pressure of 4×10^{-8} Pa. The XPS survey spectrum [Fig. 2(c)] indicates a high level of carbon contamination (0.1 monolayer) in addition to the core level peaks of $BiFeO_3$, i.e., one carbon atom every other unit cell. The O 1*s* spectrum (not shown) shows a main peak at 530 eV due to oxygen in the $BiFeO_3$ and a second component at 532 eV, consistent with OH or carbonate adsorbate species [31]. This supports the idea that chemical species are adsorbed on the $BiFeO_3$ surface in order to screen the surface bound charges [32]. Screening is provided by the adsorption of negatively charged species on the written domains with upward polarization, and positively charged species on the pristine background with downward polarization. Therefore this mechanism fully reverses the surface potential contrast, indicating greater than 50% screening through chemical adsorption, possibly promoted by the very high ferroelectric polarization of super-tetragonal $BiFeO_3$.

IV. TEMPERATURE DEPENDENCE OF THE SURFACE AND STRUCTURAL PROPERTIES

We now focus on the temperature dependence of the potential contrast between upward and downward polarized domains by heating the samples in situ while acquiring electron images. LEEM images of $BiFeO_3/Ca_{0.96}Ce_{0.04}MnO_3/YAlO_3$ are shown for temperatures increasing from 293 to 951 K [Fig. 3(a)]. The contrast is qualitatively the same up to 774 K with upward ferroelectric domains brighter than the surrounding downward domains, although there are subtle changes in magnitude [Fig. 3(b)], possibly related to previously observed phase transitions [15,16,33]. A contrast inversion occurs around 873 ± 50 K. The uncertainty in the temperature corresponds to the temperature steps chosen for the heating-imaging cycles. The written domains with upward polarization become darker than the surrounding as-grown film suggesting that the surface charge has changed sign. The disappearance of the domain contrast and then reappearance with opposite sign are attributed to progressive chemical desorption of screening species. When a 50% screening state is achieved for both upward and downward polarization, no potential contrast can be observed [Fig. 3(a), 818 K]. Then, if a sufficient amount of screening species is desorbed, we recover the clean $BiFeO_3$ surface and, consequently, the expected potential contrast with the downward polarized background providing a superior surface potential compared with the upward polarized squares [Figs. 3(a) and 3(b), 873 K]. This is reminiscent of what was observed by temperature-dependent KPFM by Liu *et al.* [34]. These authors report the same inverted potential contrast and normal contrast recovery after heating periodically poled $LiNbO_3$ crystals in vacuum. We checked that this contrast inversion is maintained while cooling the sample down to room temperature. This is illustrated by the LEEM images in Fig. 4. The fully screened surface is shown in Fig. 4(a), and the unscreened surface after desorption in UHV of the polar screening species is shown in Fig. 4(b). The same contrast is maintained [Fig. 4(c)] on cooling from the ferroelectric state, whereas on cooling from above the Curie temperature, i.e., from the paraelectric state, no domain contrast is observed. Indeed, the back-to-normal contrast is kept once desorption has been promoted by

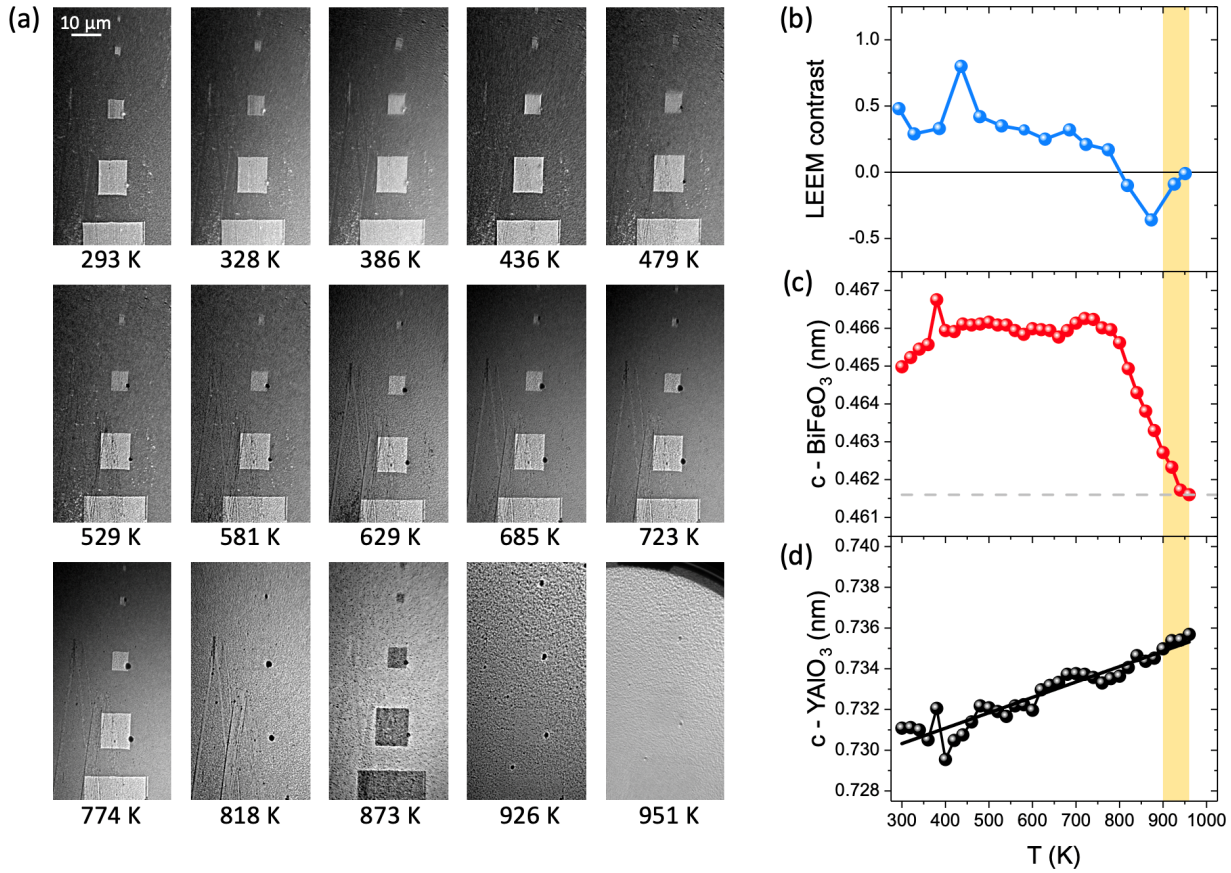

FIG. 3. (a) LEEM images of written domains in $BiFeO_3$ with polarization pointing upwards as a function of temperature. A contrast inversion occurs between 774 and 873 K. The domains disappear completely from 926 K. (b)–(d) Temperature dependencies of (b) the LEEM reflectivity contrast from (a) and of the out-of-plane lattice parameters of (c) $BiFeO_3$ and (d) $YAlO_3$ from room temperature to 960 K. While the lattice constant of $YAlO_3$ (black circles) increases linearly, that of $BiFeO_3$ (red circles) starts decreasing abruptly from 800 K until 940 K. LEEM and x-ray diffraction suggest a ferroelectric-to-paraelectric phase transition around 930 ± 30 K in the film (yellow area). The jump at about 375 K is an artifact due to sample misalignment.

heating up the sample to the suitable temperature under UHV. Finally, this LEEM contrast disappears between 926 and 951 K, suggesting the onset of the ferroelectric-to-paraelectric phase transition at 930 ± 30 K. We checked that after the heating sequence, when back to room temperature, the written domains do not reappear [Fig. 4(d)] but the $BiFeO_3$ goes back to its ferroelectric state and is still switchable as it was as grown. The contrast change at 930 ± 30 K is therefore a true phase transition.

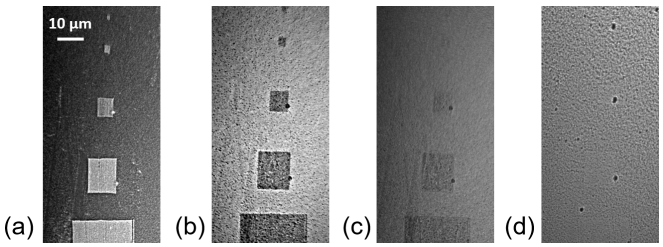

FIG. 4. LEEM images of written domains in $BiFeO_3$ with polarization pointing upwards at (a) room temperature; (b) 873 K, after desorption of screening species; (c) 382 K, after cooling in UHV from 873 K; and (d) room temperature after cooling from above the Curie temperature.

In order to validate the relevance of this "surface-sensitive" LEEM approach to assess the ferroelectric state, we performed temperature-dependent "bulk-sensitive" x-ray diffraction experiments on a similar sample. 2θ-ω diffraction scans are acquired from room temperature up to 960 K around the $BiFeO_3$ (001) and $YAlO_3$ (002) peaks. The out-of-plane parameter of $BiFeO_3$ slightly increases from room temperature to 400 K and then remains roughly constant up to 800 K with values of 0.466 ± 0.001 nm [Fig. 3(c)]. Then it sharply decreases down to 0.462 nm at 940 K. On the other hand, the out-of-plane lattice parameter of the $YAlO_3$ substrate linearly increases with temperature [Fig. 3(d)], characteristic of simple thermal expansion. Thus the sharp decrease of the out-of-plane lattice of $BiFeO_3$ is indicative of a phase transition. If we consider that the in-plane parameter of $BiFeO_3$ is initially as measured from reciprocal space mapping [Fig. 1(b)] and follows the thermal expansion of the $YAlO_3$ substrate, we can estimate the variation of the c/a tetragonality with temperature. The calculated c/a first increases from 1.225 at room temperature to 1.230 at 400 K and then slowly decays to 1.223 at 800 K. The change of behavior at 400 K is in line with the subtle changes we also observed at about this temperature in the LEEM contrast [Fig. 3(b)] and may be the signature of previously reported phase transitions [15,16,32]. Between

800 and 960 K, the tetragonality decreases to 1.209. The transition occurs over a wide temperature range and may be related to the misfit strain which varies with temperature. The difference between the low-temperature c/a ratio and that at 960 K is around 1.5%, which is typical of a ferroelectric-paraelectric phase transition. Interestingly, at this phase transition, the super-tetragonal phase does not become cubic but takes on a tetragonally distorted centrosymmetric phase due the high compressive strain. Reciprocal space mappings at high temperature would be required to gain more insights into the paraelectric phase symmetry. We suggest that epitaxial strain in homogeneities or strain gradients are at the root of the wide temperature range (150 K) over which we observe the strong decrease in the c/a ratio. These temperature-dependent x-ray diffraction experiments thus confirm that the disappearance of the potential contrast between upward and downward domains observed by LEEM at 926 K [Fig. 3(a)] is due to the ferroelectric-paraelectric transition in the super-tetragonal $BiFeO_3$ films.

V. CONCLUSION

In summary, we investigated the temperature evolution of the ferroelectric properties of super-tetragonal $BiFeO_3$ thin films grown on $YAlO_3$ using surface-sensitive low-energy electron microscopy. Micrometer-sized ferroelectric domains were defined by piezoresponse force microscopy and subsequently observed by low-energy electron microscopy from room temperature to 950 K. The surface reflectivity of upward polarized domains is higher than for downward ones at room temperature. This observation is supported by Kelvin probe force microscopy, showing a lower surface potential for the written upward domains than for the as-grown downward domains. We interpret this counterintuitive result by the fact that over 50% polar screening species are present at the surface of the ferroelectric thin film. With increasing temperature, the contrast between up and down domains reverses at 873 ± 50 K when surface adsorbates desorb to reveal a surface charge that is consistent with unscreened surface polarization charge. Finally, we determine the Curie temperature of the film when the contrast between up and down domains vanishes at 930 ± 30 K. The surface-sensitive detection of the Curie temperature is confirmed by bulk temperature-dependent x-ray diffraction experiments. These experiments indicate that the Curie temperature of the super-tetragonal polymorph of $BiFeO_3$ is significantly distinct from its parent compound and demonstrate that low-energy electron microscopy can provide insights into ferroelectric phase transitions of ultrathin films. The results provide a better understanding of the phase diagram of highly strained $BiFeO_3$ in view of potential applications and reveal the importance of surface screening in defining the boundary conditions on the ferroelectric film.

ACKNOWLEDGMENTS

We thank Daniel Sando for fruitful discussions. We acknowledge support from the French Agence Nationale de la Recherche (ANR) through the FERROMON project and the DFG-ANR 2014 project HREELM (Grant No. ANR-14-CE35-0019-03). This work was supported by a public grant overseen by the ANR as part of the Investissement d'Avenir program (LABEX NanoSaclay, Grant No. ANR-10-LABX-0035). We also thank the LABEX NanoSaclay for the Wall-Co project.

[1] R. T. Smith, G. D. Achenbach, R. Gerson, and W. J. James, J. Appl. Phys. (Melville, NY) **39**, 70 (1968).
[2] J. M. Moreau, C. Michel, R. Gerson, and W. J. James, J. Phys. Chem. Solids **32**, 1315 (1971).
[3] G. Catalan and J. F. Scott, Adv. Mater. (Weinheim) **21**, 2463 (2009).
[4] D. Lebeugle, D. Colson, A. Forget, and M. Viret, Appl. Phys. Lett. **91**, 22903 (2007).
[5] J. T. Heron, J. L. Bosse, Q. He, Y. Gao, M. Trassin, L. Ye, J. D. Clarkson, C. Wang, J. Liu, S. Salahuddin, D. C. Ralph, D. G. Schlom, J. Íñiguez, B. D. Huey, and R. Ramesh, Nature (London) **516**, 370 (2014).
[6] L. Yin and W. Mi, Nanoscale **12**, 477 (2020).
[7] H. Béa, B. Dupé, S. Fusil, R. Mattana, E. Jacquet, B. Warot-Fonrose, F. Wilhelm, A. Rogalev, S. Petit, V. Cros, A. Anane, F. Petroff, K. Bouzehouane, G. Geneste, B. Dkhil, S. Lisenkov, I. Ponomareva, L. Bellaiche, M. Bibes, and A. Barthélémy, Phys. Rev. Lett. **102**, 217603 (2009).
[8] J. X. Zhang, Q. He, M. Trassin, W. Luo, D. Yi, M. D. Rossell, P. Yu, L. You, C. H. Wang, C. Y. Kuo, J. T. Heron, Z. Hu, R. J. Zeches, H. J. Lin, A. Tanaka, C. T. Chen, L. H. Tjeng, Y.-H. Chu, and R. Ramesh, Phys. Rev. Lett. **107**, 147602 (2011).
[9] Z. Fan, J. Xiao, H. Liu, P. Yang, Q. Ke, W. Ji, K. Yao, K. P. Ong, K. Zeng, and J. Wang, ACS Appl. Mater. Interfaces **7**, 2648 (2015).
[10] D. Sando, B. Xu, L. Bellaiche, and V. Nagarajan, Appl. Phys. Rev. **3**, 011106 (2016).
[11] R. J. Zeches, M. D. Rossell, J. X. Zhang, A. J. Hatt, Q. He, C.-H. Yang, A. Kumar, C. H. Wang, A. Melville, C. Adamo, G. Sheng, Y.-H. Chu, J. F. Ihlefeld, R. Erni, C. Ederer, V. Gopalan, L. Q. Chen, D. G. Schlom, N. A. Spaldin, L. W. Martin *et al.*, Science **324**, 977 (2009).
[12] D. Sando, Y. Yang, E. Bousquet, C. Carrétéro, V. Garcia, S. Fusil, D. Dolfi, A. Barthélémy, P. Ghosez, L. Bellaiche, and M. Bibes, Nat. Commun. **7**, 10718 (2016).
[13] H. Yamada, V. Garcia, S. Fusil, S. Boyn, M. Marinova, A. Gloter, S. Xavier, J. Grollier, E. Jacquet, C. Carrétéro, C. Deranlot, M. Bibes, and A. Barthélémy, ACS Nano **7**, 5385 (2013).
[14] S. Boyn, J. Grollier, G. Lecert, B. Xu, N. Locatelli, S. Fusil, S. Girod, C. Carrétéro, K. Garcia, S. Xavier, J. Tomas, L. Bellaiche, M. Bibes, A. Barthélémy, S. Saighi, and V. Garcia, Nat. Commun. **8**, 14736 (2017).
[15] C. Beekman, W. Siemons, T. Z. Ward, M. Chi, J. Howe, M. D. Biegalski, N. Balke, P. Maksymovych, A. K. Farrar, J. B. Romero, P. Gao, X. Q. Pan, D. A. Tenne, and H. M. Christen, Adv. Mater. (Weinheim) **25**, 5561 (2013).
[16] H. J. Liu, H. J. Chen, W. I. Liang, C. W. Liang, H. Y. Lee, S. J. Lin, and Y. H. Chu, J. Appl. Phys. (Melville, NY) **112**, 052002 (2012).

[17] W. Siemons, M. D. Biegalski, J. H. Nam, and H. M. Christen, Appl. Phys. Express **4**, 095801 (2011).
[18] S. V. Kalinin and D. A. Bonnell, Appl. Phys. Lett. **78**, 1116 (2001).
[19] G. Geneste and B. Dkhil, Phys. Rev. B **79**, 235420 (2009).
[20] J. L. Wang, F. Gaillard, A. Pancotti, B. Gautier, G. Niu, B. Vilquin, V. Pillard, G. L. M. P. Rodrigues, and N. Barrett, J. Phys. Chem. C **116**, 21802 (2012).
[21] N. Domingo, I. Gaponenko, K. Cordero-Edwards, N. Stucki, V. Pérez-Dieste, C. Escudero, E. Pach, A. Verdaguer, and P. Paruch, Nanoscale **11**, 17920 (2019).
[22] A. N. Morozovska, E. A. Eliseev, N. V. Morozovsky, and S. V. Kalinin, Phys. Rev. B **95**, 195413 (2017).
[23] L. Xie, L. Li, C. A. Heikes, Y. Zhang, Z. Hong, P. Gao, C. T. Nelson, F. Xue, E. Kioupakis, L. Chen, D. G. Schlom, P. Wang, and X. Pan, Adv. Mater. (Weinheim) **29**, 1701475 (2017).
[24] X. Li, Q. Zhu, L. Vistoli, A. Barthélémy, M. Bibes, S. Fusil, V. Garcia, and A. Gloter, Adv. Mater. Interfaces **7**, 2000601 (2020).
[25] J. E. Rault, W. Ren, S. Prosandeev, S. Lisenkov, D. Sando, S. Fusil, M. Bibes, A. Barthélémy, L. Bellaiche, and N. Barrett, Phys. Rev. Lett. **109**, 267601 (2012).
[26] N. Barrett, J. Rault, J. Wang, C. Mathieu, A. Locatelli, T. Mentes, M. Niño, S. Fusil, M. Bibes, A. Barthélémy, D. Sando, W. Ren, S. Prosandeev, L. Bellaiche, B. Vilquin, A. Petraru, I. Krug, and C. Schneider, J. Appl. Phys. (Melville, NY) **113**, 187217 (2013).
[27] X. Martí, P. Ferrer, J. Herrero-Albillos, J. Narvaez, V. Holy, N. Barrett, M. Alexe, and G. Catalan, Phys. Rev. Lett. **106**, 236101 (2011).
[28] S. V. Kalinin and D. A. Bonnell, Phys. Rev. B **63**, 125411 (2001).
[29] S. V. Kalinin, C. Y. Johnson, and D. A. Bonnell, J. Appl. Phys. (Melville, NY) **91**, 3816 (2002).
[30] O. Copie, N. Chevalier, G. Le Rhun, C. Rountree, D. Martinotti, S. Gonzalez, C. Mathieu, O. Renault, and N. Barrett, ACS Appl. Mater. Interfaces **9**, 29311 (2017).
[31] J. D. Baniecki, M. Ishii, T. Shioga, K. Kurihara, and S. Miyahara, Appl. Phys. Lett. **89**, 162908 (2006).
[32] L. C. Tanase, N. G. Apostol, L. E. Abramiuc, C. A. Tache, L. Hrib, L. Trupinç, L. Pintilie, and C. M. Teodorescu, Sci. Rep. **6**, 35301 (2016).
[33] I. C. Infante, J. Juraszek, S. Fusil, B. Dupé, P. Gemeiner, O. Diéguez, F. Pailloux, S. Jouen, E. Jacquet, G. Geneste, J. Pacaud, J. Íñiguez, L. Bellaiche, A. Barthélémy, B. Dkhil, and M. Bibes, Phys. Rev. Lett. **107**, 237601 (2011).
[34] X. Liu, K. Kitamura, and K. Terabe, Appl. Phys. Lett. **89**, 132905 (2006).